Original Article

Accuracy of cone-beam breast computed tomography for assessing breast cancer tumor size—comparison with breast magnetic resonance imaging

Mengran Zhao[1#], Xiangchao Song[1#], Yue Ma[1], Zhijun Li[1], Yafei Wang[1], Aidi Liu[1], Hong Lu[2], Ying Ma[3], Zhaoxiang Ye[1]

[1]Department of Radiology, Tianjin Medical University Cancer Institute & Hospital, National Clinical Research Center for Cancer, Tianjin's Clinical Research Center for Cancer, Key Laboratory of Breast Cancer Prevention and Therapy, Tianjin Medical University, Ministry of Education, Key Laboratory of Cancer Prevention and Therapy, Tianjin, China; [2]Department of Breast Imaging, Tianjin Medical University Cancer Institute & Hospital, National Clinical Research Center for Cancer, Tianjin's Clinical Research Center for Cancer, Key Laboratory of Breast Cancer Prevention and Therapy, Tianjin Medical University, Ministry of Education, Key Laboratory of Cancer Prevention and Therapy, Tianjin, China; [3]Department of Pancreatic Cancer, Tianjin Medical University Cancer Institute & Hospital, National Clinical Research Center for Cancer, Tianjin's Clinical Research Center for Cancer, Key Laboratory of Breast Cancer Prevention and Therapy, Tianjin Medical University, Ministry of Education, Key Laboratory of Cancer Prevention and Therapy, Tianjin, China

Contributions: (I) Conception and design: M Zhao, X Song; (II) Administrative support: H Lu, Z Ye; (III) Provision of study materials or patients: M Zhao, X Song; (IV) Collection and assembly of data: M Zhao, X Song, Yue Ma, Y Wang; (V) Data analysis and interpretation: M Zhao, Yue Ma, Y Wang, A Liu; (VI) Manuscript writing: All authors; (VII) Final approval of manuscript: All authors.

[#]These authors contributed equally to this work as co-first authors.

Correspondence to: Zhaoxiang Ye, MD. Department of Radiology, Tianjin Medical University Cancer Institute & Hospital, National Clinical Research Center for Cancer, Tianjin's Clinical Research Center for Cancer, Key Laboratory of Breast Cancer Prevention and Therapy, Tianjin Medical University, Ministry of Education, Key Laboratory of Cancer Prevention and Therapy, Huan-Hu-Xi Road, Ti-Yuan-Bei, Hexi District, Tianjin 300060, China. Email: zye@tmu.edu.cn.

Background: Accurate preoperative assessment of tumor size is important in developing a surgical plan for breast cancer. The purpose of this study was to evaluate the accuracy of cone-beam breast computed tomography (CBBCT) and magnetic resonance imaging (MRI) in the assessment of tumor size and to analyze the factors influencing the discordance.

Methods: In this retrospective study, patients with breast cancer who underwent preoperative contrast-enhanced CBBCT (CE-CBBCT) and dynamic contrast-enhanced MRI (DCE-MRI) and received a complete pathologic diagnosis from August 2020 to December 2021 were included, using the pathological result as the gold standard. Two radiologists assessed the CBBCT and MRI features and measured the tumor size with a 2-week washout period. Intraclass correlation coefficient (ICC) and Bland-Altman analyses were used to assess inter-observer reproducibility and agreement based on CBBCT, MRI and pathology. Univariate analyses of differences in clinical, pathological and CBBCT/MRI features between the concordant and discordant groups was performed using the *t*-test, Mann-Whitney *U*-test, Chi-squared test and Fisher's exact test. Multivariate analyses were used to identify factors associated with discordance of CBBCT/MRI with pathology.

Results: A total of 115 female breast cancer patients (115 lesions) were included. All patients had a single malignant tumor of the unilateral breast. The reproducibility and the agreement ranged from moderate to excellent (ICC =0.607–0.983). Receiver operating characteristic (ROC) analyses showed that the cut-off values of CBBCT-pathology and MRI-pathology discordance were 2.25 and 2.65 cm, respectively. CBBCT/MRI-pathology concordance was significantly associated with the extent of pathology, lesion type, presence of calcification, human epidermal growth factor receptor 2 (HER2) status and fatty infiltration (P<0.05). In lesions containing calcification, the difference of CBBCT-pathology was significantly smaller than MRI-pathology (P=0.021). Non-mass enhancement (NME) was the main predictor of CBBCT- or MRI-pathology

discordance [odds ratio (OR) =3.293–6.469, P<0.05], and HER2 positivity was a predictor of CBBCT-pathology discordance (OR =3.514, P=0.019).

Conclusions: CBBCT and MRI have comparable accuracy in measurement of tumor size, and CBBCT is advantageous in assessing the size of calcified lesions. NME and HER2 positivity are significant predictors of CBBCT-pathology discordance. This suggests that CBBCT might serve as an alternative imaging technique to assess tumor size when patients do not tolerate MRI.

Keywords: Cone-beam breast computed tomography (CBBCT); magnetic resonance imaging (MRI); tumor size; pathology

Submitted Sep 24, 2023. Accepted for publication Jan 23, 2024. Published online Mar 22, 2024.
doi: 10.21037/gs-23-401
View this article at: https://dx.doi.org/10.21037/gs-23-401

Introduction

Surgical excision is one of the main clinical treatment modalities for breast tumors (1,2). For patients with breast cancer, radical mastectomy allows complete removal of the lesion in order to prevent recurrence of the malignant disease (3). At the same time, however, the extensive trauma of this invasive procedure can have a significant impact on the patient's quality of life and aesthetic needs after surgery. With the development of precision therapy and integrated systemic treatment, breast-conserving surgery (BCS) has been increasingly relied on by patients and surgeons in recent years (4-6). An extensive tumor is one of the main factors that can make BCS unfeasible or unsuccessful. Therefore, an accurate preoperative assessment of tumor size is important in the planning of breast cancer surgery (7,8).

Radiological techniques play a crucial role in the pretreatment assessment of breast cancer, with breast magnetic resonance imaging (MRI) considered to be the most sensitive imaging technique available (9,10). MRI has high soft tissue resolution (11) and measures tumor size more accurately than mammography or ultrasound (12). However, due to the limitations of imaging principles, MRI cannot show calcifications in a breast cancer lesion, which are often a sign of ductal carcinoma *in situ* (13). The inability of MRI to detect calcifications can lead to a false assessment of tumor size, resulting in failure of BCS and an increased rate of reoperation.

Cone-beam breast computed tomography (CBBCT) is a new breast imaging technique in which its diagnostic sensitivity is comparable to that of MRI and allows a faster acquisition speed (14,15). Enhanced imaging using an injected iodine-containing contrast agent can reveal morphological features, calcification features and hemodynamic features of lesions, making it a promising complementary imaging approach for the breast. In several previous studies, CBBCT has shown encouraging results for the diagnosis of suspicious calcifications in the breast (16), the assessment of background parenchymal enhancement (BPE) (17), and the prediction of molecular subtypes of breast cancer (18-20). Consequently, the diagnostic capabilities of CBBCT are considered comparable to those of MRI in the preoperative evaluation of breast tumors (21,22). CBBCT may be a reliable alternative for assessing the extent of lesions when patients cannot undergo MRI

Highlight box

Key findings

- Cone-beam breast computed tomography (CBBCT) and magnetic resonance imaging (MRI) have comparable accuracy in measurement of tumor size, and CBBCT is advantageous in assessing the size of calcified lesions.

What is known and what is new?

- Breast MRI is currently considered the most sensitive radiological technique in the diagnosis and preoperative evaluation of breast cancer.
- CBBCT is a new breast imaging technique of which the diagnostic sensitivity is comparable to that of MRI.

What is the implication, and what should change now?

- Our findings suggest that CBBCT- and MRI-based measurements of breast lesion size have comparable accuracy, and CBBCT is superior in assessing the size of breast lesions that contain calcification. These findings provide important insights into the utility of CBBCT in the preoperative evaluation of breast cancer, namely, that CBBCT may be an alternative to MRI for assessing tumor size when patients are intolerant to MRI.

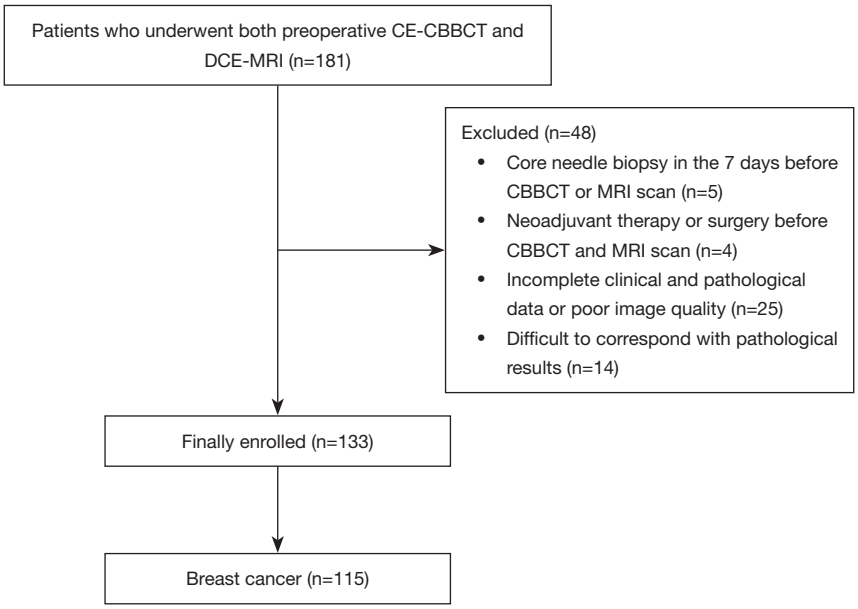

Figure 1 Flow chart of patient selection and exclusion. CE-CBBCT, contrast-enhanced CBBCT; CBBCT, cone-beam breast computed tomography; DCE-MRI, dynamic contrast-enhanced MRI; MRI, magnetic resonance imaging.

for reasons such as contraindications. However, much of the research to date has focused on the factors that lead to discordance between MRI and pathological measurements of tumor size (8,23), while little attention has been paid to the use of CBBCT for tumor size assessment.

Therefore, the main objectives of this study were to evaluate the accuracy of CBBCT and MRI for breast cancer size assessment and to analyze the influencing factors that lead to discordance between CBBCT- and MRI-pathology assessment. We present this article in accordance with the STARD reporting checklist (available at https://gs.amegroups.com/article/view/10.21037/gs-23-401/rc).

Methods

Patients

This retrospective study initially included 181 patients who underwent both preoperative contrast-enhanced CBBCT (CE-CBBCT) and breast dynamic contrast-enhanced MRI (DCE-MRI), with the two examinations taking place no more than 2 weeks apart, over the period from August 2020 to December 2021. All patients were treated surgically, and a complete pathological diagnosis was obtained, in which immunohistochemical (IHC) receptor status was determined. The exclusion criteria were as follows: (I) core needle biopsy within 7 days prior to the CBBCT or MR scan; (II) a history of neoadjuvant or surgical therapy prior to the CBBCT or MR scan; (III) incomplete clinical or pathological data or insufficient image quality for analysis; and (IV) multifocal or multicentric lesions that were difficult to correlate with the pathological results (*Figure 1*). This study was conducted in accordance with the Declaration of Helsinki (as revised in 2013). The ethics committee of Tianjin Medical University Cancer Institute & Hospital (No. bc2016039) approved this retrospective study and waived the requirement for informed consent.

CBBCT and MRI protocols

The timing of the CBBCT and MRI examinations was not related to the menstrual cycle. The two scans were conducted more than 4 hours apart to prevent any interaction of contrast agents or increase in renal metabolic burden.

CBBCT

All CBBCT examinations were performed using a dedicated flat-panel detector breast CT system (KBCT1000, Koning Corporation, USA). During the scanning process, the patient was placed in the prone position, the breast to be examined was naturally suspended in the scanning field,

and both sides of breast were scanned alternately. After an initial non-contrast-enhanced CBBCT (NCE-CBBCT) scan, a high-pressure syringe was used to inject 90 mL of a nonionic iodinated contrast agent (Iohexol, Omnipaque® 300, GE Healthcare, USA) intravenously at a rate of 2.0 or 2.5 mL/s, followed immediately by a CE-CBBCT scan. Contrast-enhanced images of the affected breast were obtained 120 s after injection of contrast agent, and images of the contralateral breast were obtained approximately 180 s after injection, depending on the time of repositioning. The specific scanning parameters were as follows: the tube voltage was constant at 49 kVp, and the tube current was automatically adjusted according to the density and size of the breast (range, 50–80 mA). Regarding doses, unilateral breast CE-CBBCT scans entailed 11.46–14.68 mGy for most women, and scans of some large and extremely dense breasts involved 18.34 mGy. The original CBBCT images were processed by the workstation to obtain an isotropic three-dimensional stereo image; the voxel size in standard mode was 0.273 mm^3.

MRI

MRI scans were performed using a 1.5 T (GE Signa HDxt, USA) system (GE Medical Systems, USA). A four-channel phased-array breast coil was used, and patients were scanned in the prone position. DCE-MRI was obtained by volume imaging for breast assessment [VIBRANT; repetition time (TR) =6.1 ms, echo time (TE) =2.9 ms; matrix size 256×128; slice thickness =1.8 mm, field of view (FOV) =26 cm × 26 cm, flip angle =15°, number of excitation (NEX) =1]. After the mask was scanned, a gadolinium contrast agent (Meglumine Gadopentetate, Magnevist, Bayer Healthcare, Germany) was injected intravenously using an MR-specific high-pressure syringe, followed by an equal volume of normal saline. The injected dose was 0.2 mL/kg, and the rate was 2 mL/s. Immediately after the injection, five phases of sagittal contrast-enhanced images were scanned continuously, with the scanning duration of each phase being approximately 90 s. Finally, axial contrast-enhanced scanning was performed.

Pathology review

All specimens were sent to the pathology department for histopathological examination and tumor size measurement. After the tumor lesions were fully exposed, each lesion specimen was cut in the plane with the maximum cross-sectional area, and both the maximum diameter line and the vertical diameter of the section were measured. In addition, IHC analyses were performed. Hormone receptor positivity was defined as estrogen receptor (ER) or progesterone receptor (PR) positivity in more than 1% of tumor cells. Human epidermal growth factor receptor 2 (HER2) positivity was defined as a staining score of 3+ or 2+ with genotype amplification by fluorescence in situ hybridization (FISH). Regarding Ki-67, specimens with staining in more than 14% of tumor cells were classified as the high-proliferation group, and those with staining in 14% of cells or fewer were classified as the low-proliferation group. Molecular subtypes of breast cancer were classified according to IHC receptor status.

Image analyses

CBBCT and MR images were transmitted to the picture archiving and communication system (PACS) for image feature evaluation. MRI and CBBCT images were independently evaluated by two radiologists with 5 and 12 years of diagnostic breast imaging experience and 3 and 10 years of diagnostic CBBCT experience, respectively, while they were blinded to the pathological findings. In the case of an inconsistent assessment, qualitative information was discussed between the radiologists until they reached a consensus, and quantitative measurements were averaged between the two radiologists to calculate the final result. The American College of Radiology (ACR) 2013 Edition of the Breast Imaging Reporting and Data System (BI-RADS) (24) was used to analyze the features of DCE-MRI. The CBBCT feature analysis was performed with reference to the mammography and MRI content in the BI-RADS atlas. The largest section of the tumor was selected by reconstructing the three-dimensional volume of the tumor by three-dimensional maximum intensity projection (3D-MIP) reconstruction of the CE-CBBCT images and DCE-MRI images of 1st- and delayed-phase and the largest diameter was used for subsequent analyses. If both enhancement and calcification were present on CE-CBBCT, the overall extent was measured. Slice thicknesses of 0.273 and 1.8 mm were used for tumor size measurement on CE-CBBCT and MRI, respectively. Using the pathological result as the gold standard, CBBCT and MRI were considered concordant with pathology if the measurement difference was $<\pm 0.5$ cm, while they were considered discordant with pathology if the difference was $\geq \pm 0.5$ cm (23).

Table 1 The clinical characteristics of patients and lesion subtypes

Clinical and pathological characteristics	Values
Age (years)	49.63±8.26
Malignant lesions	115
Invasive ductal carcinoma	97 (84.35)
Ductal carcinoma *in situ* with microinvasion	7 (6.09)
Mucinous carcinoma	4 (3.48)
Invasive lobular carcinoma	3 (2.61)
Invasive micropapillary carcinoma	3 (2.61)
Ductal carcinoma *in situ*	1 (0.87)

Data are presented as mean ± standard deviation, n, or n (%).

Table 2 Agreement of tumor size detected between two reviewers and among CBBCT, MRI, and pathology specimens

Readers/measurement methods	ICC value (95% CI)
Reader 1 *vs.* reader 2	
CBBCT	0.983 (0.976, 0.988)
MRI	0.973 (0.983, 0.986)
CBBCT *vs.* pathology	0.673 (0.553, 0.763)
MRI *vs.* pathology	0.607 (0.453, 0.726)
CBBCT *vs.* MRI	0.956 (0.917, 0.974)
CBBCT *vs.* MRI *vs.* pathology	0.767 (0.684, 0.831)

CBBCT, cone-beam breast computed tomography; MRI, magnetic resonance imaging; ICC, intraclass correlation coefficient; CI, confidence interval.

Statistical analyses

Statistical analyses were performed using SPPS software (versions 25.0, IBM Crop). In terms of consistency analysis, the intraclass correlation coefficient (ICC) was calculated to assess the inter-observer agreement between the two reviewers and the consistency of the maximum diameter measured by CBBCT, MRI, and pathology. The ICC values were divided into three categories: poor (ICC <0.5), moderate (0.5≤ ICC <0.8) and excellent (ICC ≥0.8) (25). Bland-Altman analyses were used to assess the consistency of tumor size measurements based on CBBCT, MRI and pathology. Receiver operating characteristic (ROC) curve analyses were carried out to calculate the cut-off points where CBBCT/MRI differed from pathology. For difference analysis, the Kolmogorov-Smirnov test was used to analyze the normality of continuous variables firstly. The differences in clinical factors, pathological factors and CBBCT/MRI features between the concordant and discordant groups were statistically analyzed by Student's *t*-test, the Mann-Whitney *U* test, Chi-squared test and Fisher's exact test. Two-sided P values less than 0.05 were considered statistically significant. Factors that were statistically significant in the univariate analyses were subjected to multivariate analyses. Binary logistic regression was performed to identify factors associated with discordance of CBBCT/MRI pathology, and the odds ratios (ORs) and corresponding 95% confidence intervals (95% CIs) were used to assess the strength of the association of the factors.

Results

Baseline clinical and pathological characteristics

A total of 115 breast cancer patients (115 lesions) with a mean age of 49.63±8.26 years were included in this study. The patients were all female. All patients had a single malignant tumor of the unilateral breast. *Table 1* displays the summary for the clinical characteristics of patients and breast cancer subtypes.

Interobserver reproducibility and consistency between CBBCT, MRI, and pathology

Based on ICC analyses, the agreement of tumor size measurements by the two reviewers based on both CBBCT and MRI was excellent, with ICC values of 0.983 (95% CI: 0.976, 0.988) and 0.973 (95% CI: 0.983, 0.986), respectively. The agreement between CBBCT and MRI was also excellent, with ICC values of 0.956 (95% CI: 0.917, 0.974). The ICC values of 0.673 (95% CI: 0.553, 0.763) for CBBCT-pathology and 0.607 (95% CI: 0.453, 0.726) for MRI-pathology reflected moderate levels of agreement in both cases. In addition, the agreement between CBBCT, MRI and pathology reached a moderate level with an ICC value of 0.767 (95% CI: 0.684, 0.831). The results of the ICC analyses are presented in *Table 2*. Bland-Altman analyses of the tumor size measured by CBBCT, MRI and pathology are detailed in *Figure 2*, where the mean difference between CBBCT pathology was 0.37 (95% CI: −1.97, 2.70) cm, the mean difference between MRI pathology was 0.61 (95% CI: −2.17, 3.40) cm and the mean CBBCT-MRI difference was 0.25 (95% CI: −0.78, 1.27) cm.

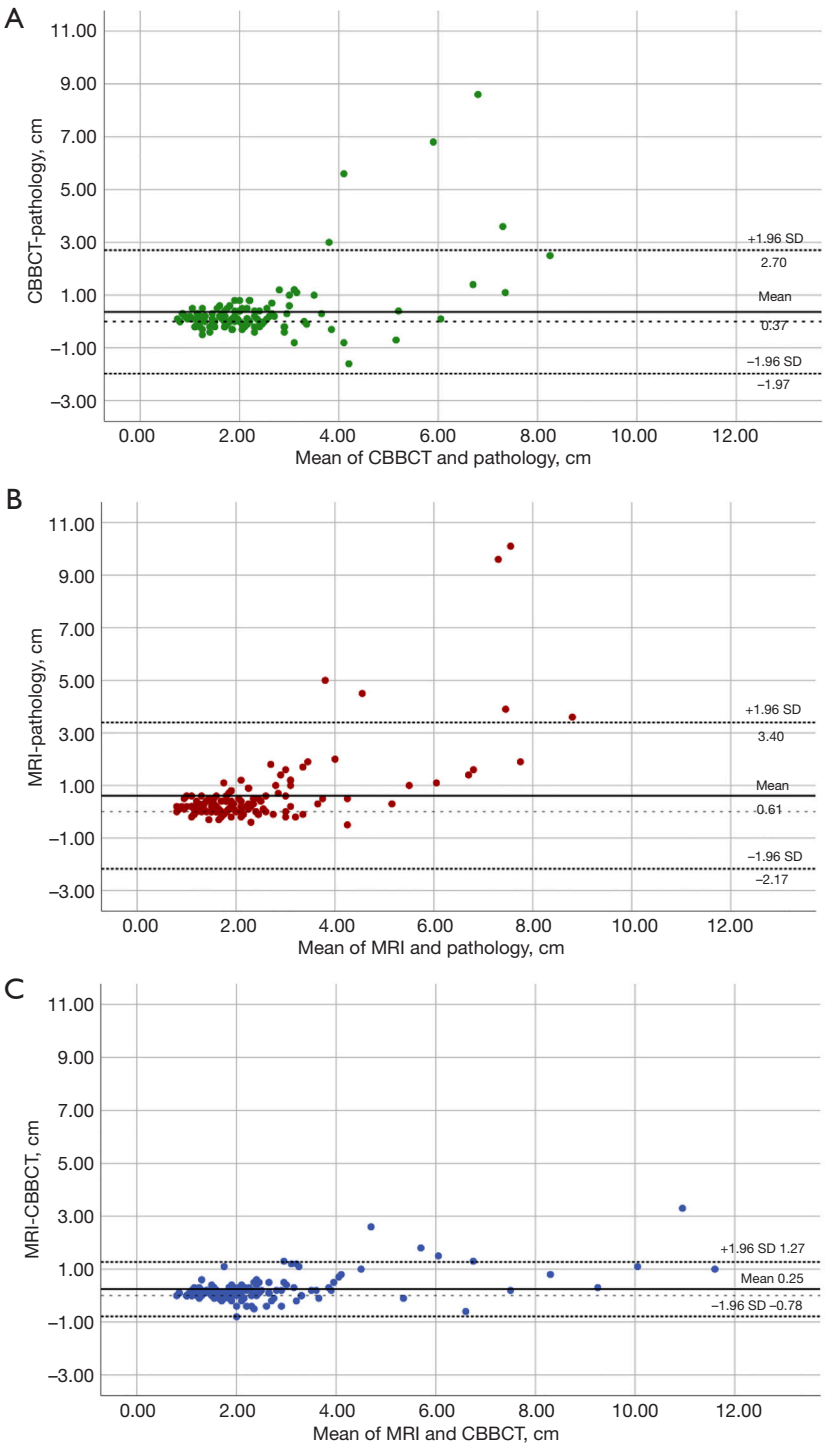

Figure 2 Bland-Altman analyses of the tumor size measured by CBBCT, MRI and pathology. Mean indicates the mean of the difference (cm), +1.96 SD and –1.96 SD indicate the 95% confidence interval of the difference (cm). CBBCT, cone-beam breast computed tomography; SD, standard deviation; MRI, magnetic resonance imaging.

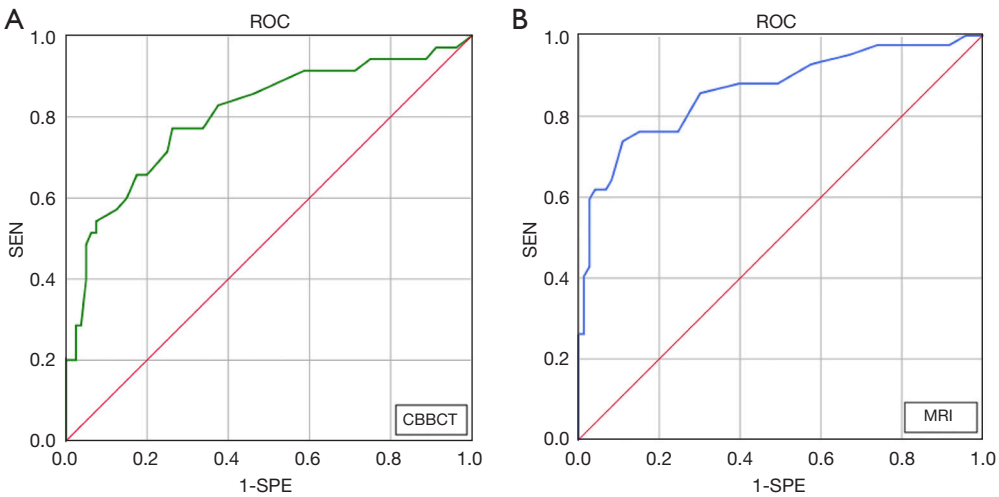

Figure 3 ROC curves based on CBBCT (A) and MRI (B) to measure the maximum diameter of the breast cancer. The results showed that the cut-off point was 2.25 cm for CBBCT-based measurements (AUC: 0.804, 95% CI: 0.710, 0.898) and 2.65 cm for MRI-based measurements (AUC: 0.864, 95% CI: 0.790, 0.939). CBBCT, cone-beam breast computed tomography; ROC, receiver operator characteristic; SPE, specificity; SEN, sensitivity; MRI, magnetic resonance imaging; AUC, area under the curve; CI, confidence interval.

Accuracy based on CBBCT and MRI measurements

Of the 115 breast cancer lesions included in this study, a total of 80 (69.6%, 80/115) were in the concordant group and 35 (30.4%, 35/115) were in the discordant group when measured by CBBCT, while a total of 73 (63.5%, 73/115) were in the concordant group and 42 (36.5%, 42/115) were in the discordant group when measured by MRI. Although CBBCT (69.6%) was slightly more accurate than MRI (63.5%), the difference was not significant (P=0.328). ROC curves were plotted with pathological tumor size as the independent variable and agreement between CBBCT- or MRI-pathology as the dependent variable (*Figure 3*). The results showed that the cut-off point was 2.25 cm for CBBCT-based measurements [area under the curve (AUC): 0.804, 95% CI: 0.710, 0.898] and 2.65 cm for MRI-based measurements (AUC: 0.864, 95% CI: 0.790, 0.939), suggesting that preoperative CBBCT and MRI assessments of tumor size tended to disagree with pathological findings when the maximum diameter was greater than 2.25 and 2.65 cm, respectively.

Factors affecting the accuracy of CBBCT/MRI-based tumor size measurement

Of the 115 breast cancers included in this study, 80 (69.6%, 80/115) were in the concordant group and 35 (30.4%, 35/115) were in the discordant group based on CBBCT measurement. Lesions in the discordant group had a greater pathological maximum diameter than those in the concordant group [2.3 (1.6, 2.9) *vs.* 1.8 (1.4, 2.2) cm, P=0.005]. HER2-positive breast cancers were more frequently found in the discordant group than in the concordant group [37.1% (13/35) *vs.* 13.8% (11/80), P=0.005]. In terms of CBBCT features, a higher proportion of lesions in the discordant group than in the concordant group exhibited non-mass enhancement (NME) [48.6% (17/35) *vs.* 13.8% (11/80), P<0.001] (*Figure 4A*), and lesions in the discordant group were also more likely to show calcifications [62.9% (22/35) *vs.* 37.5% (30/80), P=0.012] (*Figure 4B*).

Based on MRI measurements of breast cancer tumor size, a total of 73 lesions (63.5%, 73/115) were classified in the concordant group, and 42 lesions (36.5%, 42/115) were classified in the discordant group. The pathological maximum diameter of breast cancers was larger in the discordant group than in the concordant group [2.3 (1.6, 2.9) *vs.* 1.8 (1.4, 2.2) cm, P=0.002]. Fatty infiltration was more frequently observed in the concordant group than in the discordant group [84.9% (62/73) *vs.* 69.0% (29/42)]. In terms of MRI features, 50.0% (21/42) of breast cancers in the discordant group exhibited NME, whereas the vast majority of the concordant group exhibited mass-type lesions (90.4%, 66/73) (P<0.001) (*Figure 4A*).

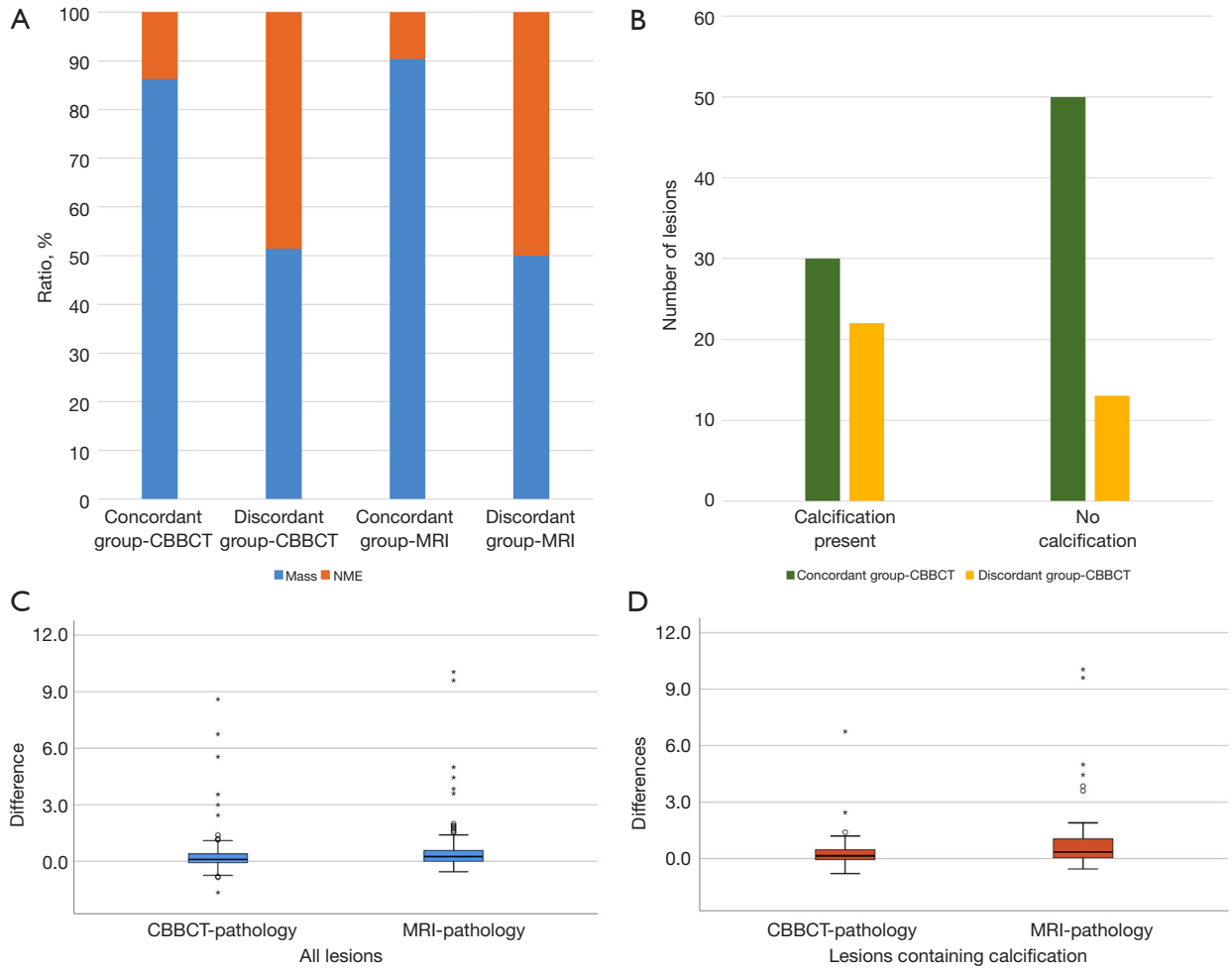

Figure 4 Representative distribution of significant clinicopathological and CBBCT/MRI features in distinguishing between concordant and discordant groups: (A) bar graph of lesion type (P<0.001); (B) bar graph of calcification in CBBCT (P=0.012); (C) boxplot of CBBCT-pathology and MRI-pathology differences in all lesions (P=0.008); (D) boxplot of CBBCT-pathology and MRI-pathology differences in lesions containing calcification (P=0.021). CBBCT, cone-beam breast computed tomography; MRI, magnetic resonance imaging; NME, non-mass enhancement.

In addition, this study compared the differences in breast cancer tumor size based on CBBCT and MRI measurements with those based on pathology specimens. Overall, the difference between CBBCT and pathology [0.1 (–0.1, 0.4) cm] was significantly smaller than that between MRI and pathology [0.3 (0.0, 0.6) cm] (P=0.008) (*Figure 4C*). In breast cancer lesions containing calcification, the difference between CBBCT and pathology was smaller than that between MRI and pathology [0.2 (–0.1, 0.5) *vs.* 0.4 (0.1, 1.0) cm, P=0.021], suggesting that CBBCT has an advantage over MRI in assessing the size of breast cancer tumors containing calcification (*Figure 4D*). *Table 3* presents the summary statistics for the univariate analyses. Example images of lesions in the concordant and discordant groups on CBBCT and MRI are shown in *Figures 5*,*6*.

Factors with significant differences in the univariate analyses were further subjected to multivariate analyses to identify factors contributing to inaccurate tumor size measurements. Multivariate analyses showed that NME (OR =4.289; 95% CI: 1.400, 13.140; P=0.011) and HER2 positivity (OR =3.514; 95% CI: 1.229, 10.045; P=0.019) were the main predictive factors for the difference between CBBCT and pathological assessment of tumor size, with NME having a stronger association. For MRI-based tumor size measurements, NME (OR =6.002; 95% CI: 2.058, 17.505; P=0.003) was also a significant predictor of

Table 3 Association of clinical, pathological and CBBCT/MRI features between the concordant and discordant groups in breast cancer (n=115)

CBBCT	CBBCT group				MRI group			
	Concordant (n=80)	Discordant (n=35)	$t/Z/\chi^2$	P value	Concordant (n=73)	Discordant (n=42)	$t/Z/\chi^2$	P value
Age (years)	50.09±8.71	48.57±7.14	0.905	0.368	50.51±8.68	48.10±7.32	1.516	0.192
Pathological maximum diameter (cm)	1.8 (1.4, 2.2)	2.3 (1.6, 2.9)	–2.789	0.005*	1.8 (1.4, 2.2)	2.3 (1.6, 2.9)	–3.087	0.002*
Menstrual status			1.156	0.282			1.461	0.227
Premenopausal	43 (53.8)	15 (42.9)			39 (53.4)	19 (45.2)		
Postmenopausal/premenopausal	37 (46.3)	20 (57.1)			34 (46.6)	23 (54.8)		
Histological grades/nuclear grades			0.358	0.549			0.031	0.859
Low and intermediate	55 (68.8)	26 (74.3)			51 (69.9)	30 (71.4)		
High	25 (31.3)	9 (25.7)			22 (30.1)	12 (28.6)		
Molecular subtypes			0.002	>0.999			2.103	0.147
Luminal	69 (86.3)	31 (88.6)			66 (90.4)	34 (81.0)		
Non-luminal	11 (13.8)	4 (11.4)			7 (9.6)	8 (19.0)		
DCIS component			2.166	0.141			1.446	0.229
Present	48 (60.0)	26 (74.3)			44 (60.3)	30 (71.4)		
Absent	32 (40.0)	9 (25.7)			29 (39.7)	12 (28.6)		
ER			0.002	>0.999			2.103	0.147
–	11 (13.8)	4 (11.4)			7 (9.6)	8 (19.0)		
+	69 (86.3)	31 (88.6)			66 (90.4)	34 (81.0)		
PR			0.487	0.485			1.567	0.211
–	18 (22.5)	10 (28.6)			15 (20.5)	13 (31.0)		
+	62 (77.5)	25 (71.4)			58 (79.5)	29 (69.0)		
HER2			8.068	0.005*			2.377	0.123
–	69 (86.3)	22 (62.9)			61 (83.6)	30 (71.4)		
+	11 (13.8)	13 (37.1)			12 (16.4)	12 (28.6)		
Ki-67			1.191	0.221			0.276	0.599
Low proliferation group	12 (15.0)	2 (5.7)			8 (11.0)	6 (14.3)		
High proliferation group	68 (85.0)	33 (94.3)			65 (89.0)	36 (85.7)		
Fatty infiltration			1.807	0.179			4.073	0.044*
–	14 (17.5)	10 (28.6)			11 (15.1)	13 (31.0)		
+	66 (82.5)	25 (71.4)			62 (84.9)	29 (69.0)		
Lymph vessel invasion			0.467	0.494			0.004	0.951
–	64 (80.0)	26 (74.3)			57 (78.1)	33 (78.6)		
+	16 (20.0)	9 (25.7)			16 (21.9)	9 (21.4)		

Table 3 (*continued*)

Table 3 (*continued*)

CBBCT	CBBCT group				MRI group			
	Concordant (n=80)	Discordant (n=35)	$t/Z/\chi^2$	P value	Concordant (n=73)	Discordant (n=42)	$t/Z/\chi^2$	P value
Axillary lymph node metastasis			1.739	0.187			0.070	0.892
–	57 (71.3)	29 (82.9)			54 (74.0)	32 (76.2)		
+	23 (28.8)	6 (17.1)			19 (26.0)	10 (23.8)		
Brest density			0.000	>0.999			3.948	0.054
Non-dense	8 (10.0)	3 (8.6)			10 (13.7)	1 (2.4)		
Dense	72 (90.0)	32 (91.4)			63 (86.3)	41 (97.6)		
BPE†			3.271	0.710			0.955	0.328
Low	65 (81.3)	23 (65.7)			58 (79.5)	30 (71.4)		
High	15 (18.8)	12 (34.3)			15 (20.5)	12 (28.6)		
Lesion type			16.028	<0.001*			23.637	<0.001*
Mass	69 (86.3)	18 (51.4)			66 (90.4)	21 (50.0)		
NME	11 (13.8)	17 (48.6)			7 (9.6)	21 (50.0)		
Calcification			6.320	0.012*	–	–	–	–
Absent	50 (62.5)	13 (37.1)			–	–	–	–
Present	30 (37.5)	22 (62.9)			–	–	–	–

Data are presented as n (%), mean ± standard deviation or median (interquartile range). †, lower categories (minimal and mild) were the low BPE status group and higher categories (moderate and significant) were the high BPE status group. *, P<0.05, the differences were statistically significant. CBBCT, cone-beam breast computed tomography; MRI, magnetic resonance imaging; DCIS, ductal carcinoma in situ; ER, estrogen receptor; PR, progesterone receptor; HER2, human epidermal growth factor receptor 2; BPE, background parenchymal enhancement; NME, non-mass enhancement.

discrepancies between MRI and pathology (*Table 4*).

Discussion

Surgical excision is one of the main clinical treatments for breast cancer, and complete removal of the lesion can reduce the recurrence rate (7). Therefore, accurate assessment of breast cancer tumor size using preoperative imaging techniques is essential for the development of a rational clinical treatment plan. The results of this study showed a high level of agreement among CBBCT, MRI and pathology in measuring breast cancer tumor size, but for larger lesions, preoperative CBBCT/MRI-based measurements were prone to deviations from pathology. In addition, we found that some clinicopathological and CBBCT/MRI features of breast cancer were significantly associated with CBBCT-pathology and MRI-pathology discordance, including pathological maximum diameter, HER2 expression status, fatty infiltration, lesion type, and presence of calcification, with NME and HER2 positivity being significant predictors of CBBCT-pathology and MRI-pathology discordance in multivariate analyses.

Both enhanced CBBCT and MRI can reflect the morphological and hemodynamic characteristics of breast tumors, which makes them comparable in terms of lesion characterization and tumor size assessment (14). In this study, the inter-reader reproducibility of CBBCT and MRI for breast tumor size assessment and the agreement of CBBCT and MRI with pathology was moderate to excellent, suggesting that CBBCT may be a suitable new imaging technique for preoperative evaluation, especially in patients with contraindications to MRI.

Compared to clinical palpation and conventional mammography or ultrasound, breast MRI has superior accuracy in measuring the extent of newly diagnosed breast cancer (26-28). Previous studies have shown that

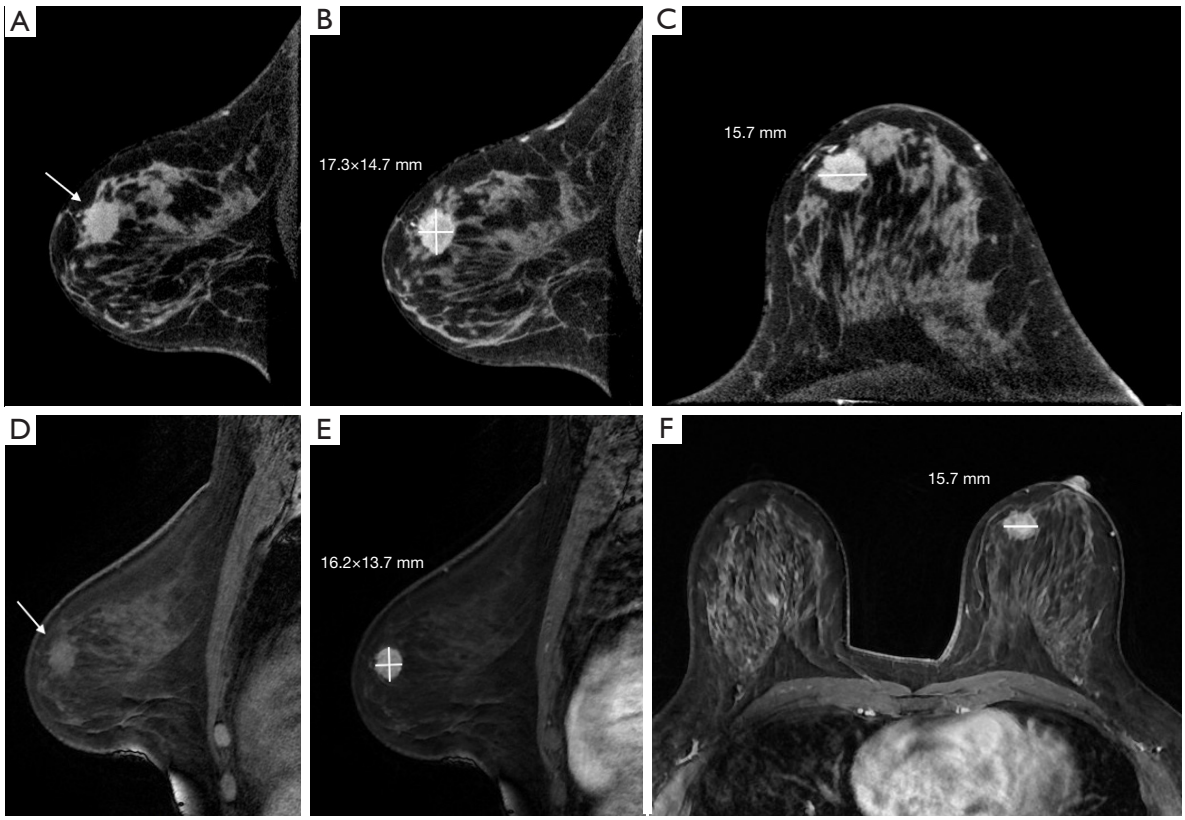

Figure 5 A 48-year-old female patient with a diagnosis of malignancy (invasive micropapillary carcinoma with invasive ductal carcinoma). The pathological maximum diameter was 1.8 cm, based on both CBBCT and MRI measurements in a concordant group. (A) A sagittal NCE-CBBCT image of a lesion presenting as a mass (arrow). A sagittal (B) and axial (C) CE-CBBCT image with a maximum lesion diameter of 1.7 cm was measured. (D) A sagittal pre-enhanced MRI image of a lesion presenting as a mass (arrow). A sagittal post-enhanced 1st phase (E) and axial delay phase (F) post-enhanced MRI image with a maximum lesion diameter of 1.6 cm was measured. CBBCT, cone-beam breast computed tomography; MRI, magnetic resonance imaging; NCE-CBBCT, non-contrast-enhanced CBBCT; CE-CBBCT, contrast-enhanced CBBCT.

the accuracy of MRI for measuring the extent of breast lesions could range from 50% (where a difference of <1 cm was classified as consistent) to 80% (where a difference of <0.5 cm was classified as consistent) (29). Discordance between MRI and pathology is often associated with larger tumor sizes, and usually MRI measurements are most accurate for tumors smaller than 2.0 cm (12,30-32). Our study showed similar results to this. Another important finding of this study is that CBBCT also had a relatively high accuracy rate (69.6%) in measuring breast tumor size, while tumors with a maximum diameter greater than 2.25 cm were prone to bias. This finding also agrees with our earlier observations (18). However, further work is required to compare the accuracy of CBBCT and MRI on a larger data set.

In addition, we found that the discrepancy between CBBCT and pathology was significantly smaller than that between MRI and pathology, and this performance may be related to the display of BPE on CE-CBBCT and DCE-MRI. Following contrast injection, enhancement of normal fibrous glandular tissue of the bilateral breast, known as BPE, may obscure the lesion or show similar enhancement, thus reducing the accuracy of tumor size assessment, particularly in breasts with moderate and marked BPE (33,34). The results of Ma *et al.* (17) confirmed that in most cases, CE-CBBCT tended to show lower BPE levels than DCE-MRI. Thus, tumor size measurement based on CE-CBBCT was less influenced by BPE than DCE-MRI, and the accuracy of measurement was higher as well.

Several previous studies have shown that NME is

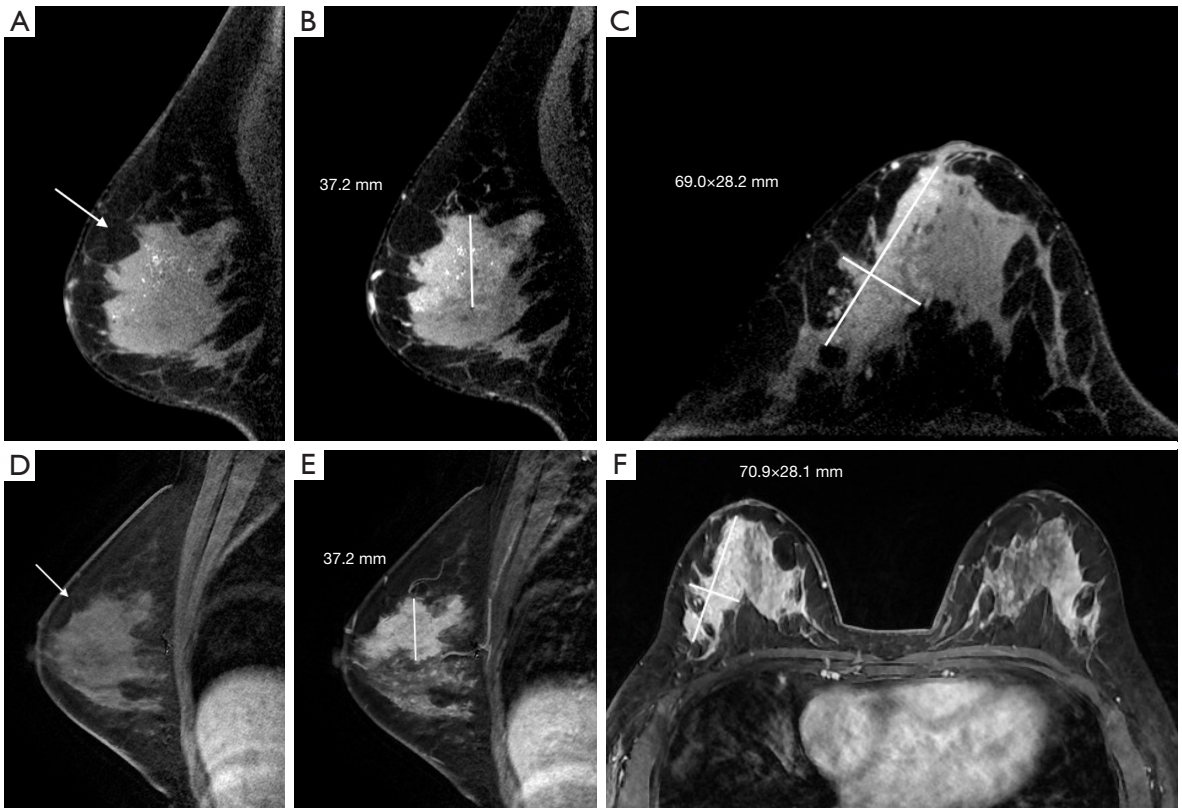

Figure 6 A 45-year-old female patient with a diagnosis of malignancy (invasive ductal carcinoma with extensive intraductal components). The pathological maximum diameter was 6.0 cm, based on both CBBCT and MRI measurements in a discordant group. (A) A sagittal NCE-CBBCT image of a lesion presenting as segmental distribution of fine polymorphic calcifications (arrow). Sagittal (B) and axial (C) CE-CBBCT images of a lesion presenting as NME, with a measured maximum diameter of 6.9 cm. (D) A sagittal pre-enhanced MRI image of a lesion that is not clearly shown (arrow). A sagittal post-enhanced 1st phase (E) and axial delay phase (F) post-enhanced MRI image of a lesion presenting as NME, with a measured maximum diameter of 7.1 cm. CBBCT, cone-beam breast computed tomography; MRI, magnetic resonance imaging; NCE-CBBCT, non-contrast-enhanced CBBCT; CE-CBBCT, contrast-enhanced CBBCT; NME, non-mass enhancement.

the most significant factor contributing to discordance between MRI and pathology measurements of tumor size (29,35-37). Similarly, our study found that NME was a significant predictor of discordance between CBBCT/MRI and pathology in multivariate analyses. Both on CBBCT/MRI and in pathological gross specimens, NME lesions often do not have clear borders, making it difficult to accurately measure tumor size (38). Preoperative assessment and clinical management of such lesions require additional care. Furthermore, a subset of breast cancers present with both mass and NME on CBBCT and MRI. There is often a non-malignant portion of such lesions, which some pathologists classify as multifocal, and usually only the clear mass portion of the lesion is measured, rather than the overall size of the tumor (35,38,39). Therefore, this part of these cases was excluded from this study.

The current study found that the presence of calcification was significantly associated with discordance between CBBCT and pathology, and that the CBBCT-pathology discrepancy of lesions with calcifications was significantly smaller than the MRI-pathology discrepancy. Breast cancers that show extensive segmental distribution of calcifications on mammography are usually seen as NME on DCE-MRI (40). In these lesions, although CE-CBBCT can show both calcification and enhancement features, the boundaries of the calcification area are difficult to determine when the lesion is large (41,42). The solid component of the tumor surrounding the calcification may not be clearly

Table 4 Multivariate analyses of factors influencing the discordance of CBBCT- and MRI-pathology measurements in breast cancer

Characteristics	CBBCT			MRI		
	OR	95% CI	P value	OR	95% CI	P value
Pathological maximum diameter	1.269	0.834, 1.932	0.266	1.543	0.955, 2.493	0.076
Lesion type						
Mass	Reference			Reference		
NME	4.289	1.400, 13.140	0.011*	6.002	2.058, 17.505	0.003*
Calcification						–
Absent	Reference			–	–	–
Present	1.290	0.488, 3.409	0.608	–	–	–
HER2						–
–	Reference			–	–	–
+	3.514	1.229, 10.045	0.019*	–	–	–
Fatty infiltration			–			
–	–	–	–	Reference		
+	–	–	–	0.887	0.282, 2.814	0.839

*, P<0.05, the differences were statistically significant. CBBCT, cone-beam breast computed tomography; MRI, magnetic resonance imaging; OR, odds ratio; CI, confidence interval; NME, non-mass enhancement; HER2, human epidermal growth factor receptor 2.

enhanced on CE-CBBCT, leading to discrepancies between CE-CBBCT and pathology (43,44).

The results of several studies have confirmed that HER2 expression status is an important factor in the accuracy of MRI assessment of tumor size (27). There is a significant correlation between HER2 positivity and tumor angiogenesis (36). For breast tumors with a high density of neovascularization, the extent of enhancement on MRI is often greater than the pathological size of the tumor (45). Although there are certain differences between CE-CBBCT and DCE-MRI in terms of image-forming principles and contrast material, CE-CBBCT has certain advantages in showing tumor angiogenesis, which can also reflect the hemodynamic characteristics of the lesion and changes in the tumor microenvironment (41). Therefore, the changes in tumor neovascularization caused by HER2 positivity would similarly affect the accuracy of CBBCT in measuring tumor size. This is supported by the finding in our study.

Despite the favorable results, a number of limitations need to be noted regarding the present study. First, our study is a retrospective analysis based on two radiologists at a single institution with a relatively small sample size. Expanding the sample size to multiple institutions would improve the reproducibility of the results of this study. Second, the measurement of non-mass type lesion size was a difficult task in both radiology and pathology. Automatic or semiautomatic measurement of NME lesion extent using artificial intelligence methods in future work will yield more accurate results. Third, the evaluation of tumor size based on 3D-MIP of CE-CBBCT or DCE-MRI may be able to improve the efficiency and accuracy of maximum tumor diameter measurement.

Conclusions

In conclusion, CBBCT- and MRI-based measurements of breast lesion size have comparable accuracy, and CBBCT is superior in assessing the size of breast lesions that contain calcification. These findings provide important insights into the utility of CBBCT in the preoperative evaluation of breast cancer, namely, that CBBCT may be an alternative to MRI for assessing tumor size when patients are intolerant to MRI. In addition, NME and HER2 positive status are significant influencing factors leading to discordance between CBBCT-based and pathology-based measurements of tumor size.

Acknowledgments

Funding: This work was supported by the National Key R&D Program of China (grant numbers 2021YFC2500400, 2021YFC2500402; grant numbers 2017YFC0112600, 2017YFC0112601), National Natural Scientific Foundation of China (grant number 82172025), Tianjin Science and Technology Major Project (grant number 19ZXDBSY00080), and Tianjin Key Medical Discipline (Specialty) Construction Project (grant number TJYXZDXK-009A).

Footnote

Reporting Checklist: The authors have completed the STARD reporting checklist. Available at https://gs.amegroups.com/article/view/10.21037/gs-23-401/rc

Data Sharing Statement: Available at https://gs.amegroups.com/article/view/10.21037/gs-23-401/dss

Peer Review File: Available at https://gs.amegroups.com/article/view/10.21037/gs-23-401/prf

Conflicts of Interest: All authors have completed the ICMJE uniform disclosure form (available at https://gs.amegroups.com/article/view/10.21037/gs-23-401/coif). The authors have no conflicts of interest to declare.

Ethical Statement: The authors are accountable for all aspects of the work in ensuring that questions related to the accuracy or integrity of any part of the work are appropriately investigated and resolved. The study was conducted in accordance with the Declaration of Helsinki (as revised in 2013). The ethics committee of Tianjin Medical University Cancer Institute & Hospital (No. bc2016039) approved this retrospective study and waived the requirement for informed consent.

References

1. Sanderink WBG, Caballo M, Strobbe LJA, et al. Reliability of MRI tumor size measurements for minimal invasive treatment selection in small breast cancers. Eur J Surg Oncol 2020;46:1463-70.
2. Goto M, Ryoo I, Naffouje S, et al. Image-guided surgery with a new tumour-targeting probe improves the identification of positive margins. EBioMedicine 2022;76:103850.
3. Jonczyk MM, Jean J, Graham R, et al. Surgical trends in breast cancer: a rise in novel operative treatment options over a 12 year analysis. Breast Cancer Res Treat 2019;173:267-74.
4. Koca B, Kuru B, Yuruker S, et al. Factors affecting surgical margin positivity in invasive ductal breast cancer patients who underwent breast-conserving surgery after preoperative core biopsy diagnosis. J Korean Surg Soc 2013;84:154-9.
5. McGuire KP, Santillan AA, Kaur P, et al. Are mastectomies on the rise? A 13-year trend analysis of the selection of mastectomy versus breast conservation therapy in 5865 patients. Ann Surg Oncol 2009;16:2682-90.
6. Kummerow KL, Du L, Penson DF, et al. Nationwide trends in mastectomy for early-stage breast cancer. JAMA Surg 2015;150:9-16.
7. Association of Breast Surgery at Baso 2009. Surgical guidelines for the management of breast cancer. Eur J Surg Oncol 2009;35 Suppl 1:1-22.
8. Mennella S, Garlaschi A, Paparo F, et al. Magnetic resonance imaging of breast cancer: factors affecting the accuracy of preoperative lesion sizing. Acta Radiol 2015;56:260-8.
9. Bae MS, Lee SH, Chu AJ, et al. Preoperative MR Imaging in Women with Breast Cancer Detected at Screening US. Radiology 2017;282:681-9.
10. Chilla GS, Tan CH, Xu C, et al. Diffusion weighted magnetic resonance imaging and its recent trend-a survey. Quant Imaging Med Surg 2015;5:407-22.
11. Li X, Chen Y, Liu J, et al. Cardiac magnetic resonance imaging of primary cardiac tumors. Quant Imaging Med Surg 2020;10:294-313.
12. Grimsby GM, Gray R, Dueck A, et al. Is there concordance of invasive breast cancer pathologic tumor size with magnetic resonance imaging? Am J Surg 2009;198:500-4.
13. Wang Y, Zhao M, Ma Y, et al. Accuracy of Preoperative Contrast-enhanced Cone Beam Breast CT in Assessment

of Residual Tumor after Neoadjuvant Chemotherapy: A Comparative Study with Breast MRI. Acad Radiol 2023;30:1805-15.
14. Wienbeck S, Fischer U, Luftner-Nagel S, et al. Contrast-enhanced cone-beam breast-CT (CBBCT): clinical performance compared to mammography and MRI. Eur Radiol 2018;28:3731-41.
15. Gong W, Zhu J, Hong C, et al. Diagnostic accuracy of cone-beam breast computed tomography and head-to-head comparison of digital mammography, magnetic resonance imaging and cone-beam breast computed tomography for breast cancer: a systematic review and meta-analysis. Gland Surg 2023;12:1360-74.
16. Liu A, Ma Y, Yin L, et al. Comparison of malignant calcification identification between breast cone-beam computed tomography and digital mammography. Acta Radiol 2023;64:962-70.
17. Ma Y, Liu A, Zhang Y, et al. Comparison of background parenchymal enhancement (BPE) on contrast-enhanced cone-beam breast CT (CE-CBBCT) and breast MRI. Eur Radiol 2022;32:5773-82.
18. Ma Y, Ye Z, Liu A, et al. The accuracy of tumor size evaluation on invasive breast cancer based on cone beam breast CT. Chin J Radiol 2019;53:286-91.
19. Uhlig J, Fischer U, von Fintel E, et al. Contrast Enhancement on Cone-Beam Breast-CT for Discrimination of Breast Cancer Immunohistochemical Subtypes. Transl Oncol 2017;10:904-10.
20. Wienbeck S, Fischer U, Perske C, et al. Cone-beam Breast Computed Tomography: CT Density Does Not Reflect Proliferation Potential and Receptor Expression of Breast Carcinoma. Transl Oncol 2017;10:599-603.
21. Li J, Zhong G, Wang K, et al. Tumor-to-Gland Volume Ratio versus Tumor-to-Breast Ratio as Measured on CBBCT: Possible Predictors of Breast-Conserving Surgery. Cancer Manag Res 2021;13:4463-71.
22. Wienbeck S, Uhlig J, Fischer U, et al. Breast lesion size assessment in mastectomy specimens: Correlation of cone-beam breast-CT, digital breast tomosynthesis and full-field digital mammography with histopathology. Medicine (Baltimore) 2019;98:e17082.
23. Yoo EY, Nam SY, Choi HY, et al. Agreement between MRI and pathologic analyses for determination of tumor size and correlation with immunohistochemical factors of invasive breast carcinoma. Acta Radiol 2018;59:50-7.
24. D'Orsi CJ, Sickles EA, Mendelson EB, et al. Breast Imaging Reporting & Data System (BI-RADS®). Reston, VA, USA: American College of Radiology, 2013.
25. Wang H, Zhou Y, Wang X, et al. Reproducibility and Repeatability of CBCT-Derived Radiomics Features. Front Oncol 2021;11:773512.
26. Hovis KK, Lee JM, Hippe DS, et al. Accuracy of Preoperative Breast MRI Versus Conventional Imaging in Measuring Pathologic Extent of Invasive Lobular Carcinoma. J Breast Imaging 2021;3:288-98.
27. Azhdeh S, Kaviani A, Sadighi N, et al. Accurate Estimation of Breast Tumor Size: A Comparison Between Ultrasonography, Mammography, Magnetic Resonance Imaging, and Associated Contributing Factors. Eur J Breast Health 2020;17:53-61.
28. Maimone S, Morozov AP, Li Z, et al. Recalibrating the decision for MRI-directed breast ultrasound in patients with newly diagnosed breast cancer, factors predicting sonographic success. Clin Imaging 2021;80:391-9.
29. Mann RM, Cho N, Moy L. Breast MRI: State of the Art. Radiology 2019;292:520-36.
30. Onesti JK, Mangus BE, Helmer SD, et al. Breast cancer tumor size: correlation between magnetic resonance imaging and pathology measurements. Am J Surg 2008;196:844-48; discussion 849-50.
31. Sezgın G, Apaydın M, Etıt D, et al. Tumor size estimation of the breast cancer molecular subtypes using imaging techniques. Med Pharm Rep 2020;93:253-9.
32. Haraldsdóttir KH, Jónsson Þ, Halldórsdóttir AB, et al. Tumor Size of Invasive Breast Cancer on Magnetic Resonance Imaging and Conventional Imaging (Mammogram/Ultrasound): Comparison with Pathological Size and Clinical Implications. Scand J Surg 2017;106:68-73.
33. Kuhl C. The current status of breast MR imaging. Part I. Choice of technique, image interpretation, diagnostic accuracy, and transfer to clinical practice. Radiology 2007;244:356-78.
34. DeMartini WB, Liu F, Peacock S, et al. Background parenchymal enhancement on breast MRI: impact on diagnostic performance. AJR Am J Roentgenol 2012;198:W373-80.
35. Rominger M, Berg D, Frauenfelder T, et al. Which factors influence MRI-pathology concordance of tumour size measurements in breast cancer? Eur Radiol 2016;26:1457-65.
36. Baek JE, Kim SH, Lee AW. Background parenchymal enhancement in breast MRIs of breast cancer patients: impact on tumor size estimation. Eur J Radiol 2014;83:1356-62.
37. Mann RM, Bult P, van Laarhoven HW, et al. Breast cancer

size estimation with MRI in BRCA mutation carriers and other high risk patients. Eur J Radiol 2013;82:1416-22.
38. Tot T. The diffuse type of invasive lobular carcinoma of the breast: morphology and prognosis. Virchows Arch 2003;443:718-24.
39. Gruber IV, Rueckert M, Kagan KO, et al. Measurement of tumour size with mammography, sonography and magnetic resonance imaging as compared to histological tumour size in primary breast cancer. BMC Cancer 2013;13:328.
40. Iotti V, Ragazzi M, Besutti G, et al. Accuracy and Reproducibility of Contrast-Enhanced Mammography in the Assessment of Response to Neoadjuvant Chemotherapy in Breast Cancer Patients with Calcifications in the Tumor Bed. Diagnostics (Basel) 2021;11:435.
41. Ma WM, Li J, Chen SG, et al. Correlation between contrast-enhanced cone-beam breast computed tomography features and prognostic staging in breast cancer. Br J Radiol 2022;95:20210466.
42. Zhao B, Zhang X, Cai W, et al. Cone beam breast CT with multiplanar and three dimensional visualization in differentiating breast masses compared with mammography. Eur J Radiol 2015;84:48-53.
43. Bazzocchi M, Zuiani C, Panizza P, et al. Contrast-enhanced breast MRI in patients with suspicious microcalcifications on mammography: results of a multicenter trial. AJR Am J Roentgenol 2006;186:1723-32.
44. Kuhl CK, Schrading S, Bieling HB, et al. MRI for diagnosis of pure ductal carcinoma in situ: a prospective observational study. Lancet 2007;370:485-92.
45. Moon HG, Han W, Lee JW, et al. Age and HER2 expression status affect MRI accuracy in predicting residual tumor extent after neo-adjuvant systemic treatment. Ann Oncol 2009;20:636-41.

Cite this article as: Zhao M, Song X, Ma Y, Li Z, Wang Y, Liu A, Lu H, Ma Y, Ye Z. Accuracy of cone-beam breast computed tomography for assessing breast cancer tumor size—comparison with breast magnetic resonance imaging. Gland Surg 2024;13(3):281-296. doi: 10.21037/gs-23-401